energies

MDPI

Article

A Wind–Storage Coordinated Frequency Regulation and Power Optimization Control Strategy Based on Multivariable Fuzzy Logic and Model Predictive Control

Tingting Cai and Yugang Sun *

Department of Electrical Engineering, Northeast Electric Power University, Jilin 132012, China; cynthia1@126.com
* Correspondence: syg549343262@126.com

Abstract

With the large-scale integration of wind power, modern power systems are facing reduced equivalent inertia, weakened primary frequency regulation capability, and insufficient coordination between wind turbines and energy storage during joint frequency support. To address these issues, this paper investigates a wind–storage hybrid system composed of doubly fed induction generators (DFIG) and supercapacitor energy storage and proposes a coordinated primary frequency regulation strategy combining fuzzy logic control (FLC) and model predictive control (MPC). Considering the variations in rotor kinetic energy reserve and frequency support capability under different wind speed regions, a coordinated regulation mechanism is developed for multiple operating conditions. In addition, a variable-coefficient synthetic inertia control scheme with rotor speed safety constraints is designed to adaptively adjust the turbine regulation coefficients, while an SOC-feedback-based adaptive virtual droop strategy is introduced to improve the sustained support capability of the energy storage unit. On this basis, a multi-objective model predictive control framework is established to optimize the reference power allocation between the wind turbine and the energy storage unit in a rolling manner. The proposed method is characterized by three coordinated features, namely, multi-region wind–storage frequency regulation, rotor-speed-safe adaptive support of the wind turbine and SOC-aware adaptive support of the storage unit, as well as MPC-based rolling power allocation. Simulation results show that the proposed strategy improves the frequency nadir, reduces the steady-state frequency deviation, and enhances coordinated power sharing, thereby improving the primary frequency regulation performance and overall frequency stability of the wind–storage hybrid system.

Keywords: doubly fed induction generator; energy storage; wind-storage combined frequency regulation; fuzzy logic control; model predictive control

Check for updates

Academic Editor: Chih-Ming Hong

Received: 24 March 2026
Revised: 17 April 2026
Accepted: 22 April 2026
Published: 24 April 2026

Copyright: © 2026 by the authors. Licensee MDPI, Basel, Switzerland. This article is an open access article distributed under the terms and conditions of the Creative Commons Attribution (CC BY) license.

1. Introduction

Driven by the ongoing advancement of the "dual-carbon" targets, wind power has been integrated into power systems on an increasingly large scale. Unlike conventional synchronous generators, wind turbines are interfaced with the grid through power electronic converters, which decouple rotor kinetic energy from grid frequency dynamics. Consequently, during frequency disturbances, wind turbines cannot inherently deliver inertial support in the same way as conventional units [1–4]. To enhance frequency security, modern wind turbines have gradually been endowed with frequency regulation

functions. At the same time, the fast progress of energy storage technology has created new possibilities for grid frequency support. Benefiting from its high power tracking capability [5] and rapid response, energy storage can be deployed alongside wind farms to form a wind–storage hybrid system capable of meeting frequency regulation requirements under different operating scenarios [6,7]. Nevertheless, when frequency regulation is undertaken solely by wind turbines, secondary frequency dips or rebounds may arise during the recovery stage [8]. Conversely, if energy storage alone provides frequency support, an excessively large storage capacity may be required [9], and the regulation potential of wind energy may not be fully utilized. Therefore, it is of practical importance to develop an effective coordinated control strategy for the wind–storage hybrid system so that wind turbines and energy storage can jointly participate in primary frequency regulation.

In recent years, considerable efforts have been devoted to the control strategies of wind–storage hybrid systems for primary frequency regulation. In [10], a synthetic inertia control strategy was incorporated while the wind turbine operated in maximum power point tracking mode; however, the virtual inertia coefficient was not analyzed in detail. In [11], an SOC-adaptive frequency regulation strategy was developed for wind energy storage systems under wind speed uncertainty, and the storage-side regulation capability was further improved through predictive optimization. In [12], a coordinated frequency regulation strategy for DFIG-based variable-speed wind turbines and battery energy storage systems was proposed, in which wind-speed zoning and SOC-adaptive droop control were jointly considered to improve the frequency nadir and mitigate the secondary frequency dip. In [13], the balance between energy storage charging and discharging was considered in the coordinated frequency modulation process of a wind–storage combined system. In [14], a wind–storage coordinated control strategy for inertia enhancement was proposed for high-renewable-energy power systems, showing that wind–storage coordination can effectively improve fast frequency response capability. In [15], the effective inertia margin of wind turbines in different wind speed intervals was quantified, and the turbine regulation parameters, together with storage power variation, were optimized through model predictive control. In [16], adaptive primary frequency regulation of a DFIG equipped with ultracapacitor energy storage was investigated by integrating adaptive virtual inertia and variable droop control. Nevertheless, these studies still do not fully address the coupling among multi-region operating logic, rotor-speed-safe fuzzy coefficient regulation, and upper-layer rolling power allocation. As a consequence, the complementary frequency support capability of wind turbines and energy storage cannot be fully utilized. For clarity, Table 1 summarizes the main methodological characteristics of recent representative studies on wind–storage coordinated primary frequency regulation.

Table 1. Comparison of recent representative studies on wind–storage coordinated primary frequency regulation.

Reference	Wind-Speed Awareness	Rotor-Speed Safety	SOC-Adaptive Storage	MPC-Based Allocation
[10]	Explicit	Not explicit	Partial	Not explicit
[11]	Partial	Not explicit	Explicit	Partial
[12]	Partial	Not explicit	Explicit	Not explicit
[13]	Not explicit	Not explicit	Partial	Not explicit
[14]	Not explicit	Not explicit	Partial	Not explicit
[15]	Explicit	Not explicit	Not explicit	Explicit
[16]	Not explicit	Partial	Explicit	Not explicit

To address the above limitations, this paper proposes a wind–storage coordinated primary frequency regulation strategy integrating fuzzy logic control and model predictive

control. Different from conventional methods that mainly focus on a single local control law or standalone power optimization, the proposed method aims to establish a unified coordinated framework for the wind turbine and the energy storage unit under varying operating conditions. In particular, the proposed strategy explicitly links the wind speed region, the available rotor kinetic energy margin, the storage SOC state, and the rolling power allocation process, so that frequency support performance, operational safety, and coordination between wind power and storage can be improved simultaneously.

The main contributions of this work are summarized as follows:

A coordinated frequency regulation mechanism for a wind–storage hybrid system is established under multiple wind speed regions. According to the turbine operating condition and the variation in its available frequency support capability, the respective regulation roles of the wind turbine and the energy storage unit are differentiated, which improves the operating adaptability of the coordinated control strategy.

For the wind turbine, a multivariable fuzzy synthetic inertia control strategy with rotor-speed safety attenuation is developed so that the virtual inertia and droop coefficients can be adaptively adjusted while preventing excessive kinetic energy release near the rotor-speed safety boundary. For the energy storage unit, an SOC-feedback-based adaptive virtual droop strategy is introduced to improve the sustainability of storage participation during primary frequency regulation.

On the basis of the above local control laws, an MPC-based upper-layer power allocation method is further incorporated to coordinate the reference power commands of the wind turbine and the energy storage unit in a rolling manner. In this way, the proposed method not only suppresses frequency deviation but also smooths the power transition between the two units during both the support stage and the recovery stage.

2. Materials and Methods

2.1. Frequency Response Analysis of Wind–Storage Hybrid Systems

2.1.1. Mathematical Model of the DFIG

The output mechanical power of the DFIG can be expressed as [17]:

$$P_{\mathrm{m}} = \frac{1}{2}\rho S v^3 C_{\mathrm{p}}(\lambda, \beta) \tag{1}$$

where ρ is the air density, S is the swept area of the rotor blades, v is the wind speed, and $C_{\mathrm{p}}(\lambda, \beta)$ is the power coefficient. is a nonlinear function of the blade pitch angle β and the tip-speed ratio λ, which can be expressed as:

$$\begin{cases} C_{\mathrm{p}} = 0.52\left(\frac{116}{\delta} - 0.4\beta - 5\right)e^{-\frac{21}{\delta}} + 0.0068\lambda \\ \frac{1}{\delta} = \frac{1}{\lambda + 0.08\beta} - \frac{0.035}{\beta^3 + 1} \\ \lambda = \frac{\omega R_{\mathrm{W}}}{v} \end{cases} \tag{2}$$

where δ is an introduced intermediate variable, ω is the rotor speed of the wind turbine, and R_{W} is the blade radius of the wind turbine.

When the pitch angle β remains constant, there exists an optimal tip-speed ratio λ_{opt} at which the power coefficient $C_{\mathrm{p}}(\lambda, \beta)$ reaches its maximum value, thereby enabling maximum wind energy capture under different wind speed conditions.

2.1.2. Mathematical Model of the Supercapacitor

In view of the relatively complex internal operating mechanism of supercapacitor energy storage, an equivalent simplification is required for simulation and modeling. The

simplified model can be represented by an RC unit composed of an equivalent resistance R and an ideal capacitor C, and its mathematical expression can be written as [18]:

$$U = I_c + R + \frac{1}{C}\int I_c dt \tag{3}$$

where U denotes the terminal voltage of the equivalent supercapacitor model, and I_c denotes the current of the supercapacitor.

The SOC of the supercapacitor can be expressed as:

$$S_{soc} = \frac{\frac{1}{2}CU^2}{\frac{1}{2}CU_{max}^2} = \frac{U^2}{U_{max}^2} \tag{4}$$

where U_{max} is the maximum operating voltage of the supercapacitor.

When a load disturbance occurs in the system, constraints on the SOC should be imposed to prevent overcharging or overdischarging of the supercapacitor during the charging and discharging process. It is therefore necessary to determine whether the current SOC satisfies the corresponding charging/discharging constraint conditions. The mathematical expression of the SOC constraints can be written as:

$$S_{soc.min} \leq S_{soc} \leq S_{soc.max} \tag{5}$$

where $S_{soc.min}$ and $S_{soc.max}$ denote the upper and lower operating limits of the state of charge, respectively.

To ensure reliable operation of the supercapacitor during the charging and discharging process and to prolong the service life of the energy storage device, the operating current of the storage unit is required not to exceed its rated current. During charging, when $S_{soc} > 0.9$, the supercapacitor approaches the charging limit region, and further charging should therefore be restricted. During discharging, when $S_{soc} < 0.1$, the supercapacitor approaches the discharging limit region, and further discharging should likewise be restricted.

2.1.3. Frequency Response Model of the Wind–Storage Hybrid System Based on Power Optimization

The overall structure of the wind–storage coordinated frequency regulation system adopted in this paper is shown in Figure 1. In this configuration, the wind turbine is connected to the AC bus through AC/DC and DC/AC converters, while the energy storage unit is connected to the AC bus through a bidirectional converter. In Figure 1, ΔP_G, ΔP_W, and ΔP_E denote the power increments of the conventional generating unit, wind turbine, and energy storage unit, respectively; $\Delta P_{W.ref}$ and $\Delta P_{E.ref}$ denote the reference output powers of the wind turbine and energy storage unit, respectively; and Δf denotes the grid frequency deviation.

A load disturbance in the power grid gives rise to frequency variation owing to the active power mismatch on the AC bus. On the basis of the present system frequency and its future predicted trajectory, the model predictive controller coordinates the operating states of the wind turbine and the energy storage unit to generate their respective reference power commands. Through this coordinated optimization process, the system frequency regulation performance can be improved, and the frequency support power can be distributed more appropriately between wind power and energy storage [19].

In the analysis of primary frequency regulation, the electromagnetic transient process is neglected, and a frequency response model of the wind–storage hybrid system is

established. After the power grid is subjected to a power disturbance, the corresponding frequency response equation can be expressed as:

$$\Delta f(s) = \frac{\Delta P_{\mathrm{G}}(s) + \Delta P_{\mathrm{W}}(s) + \Delta P_{\mathrm{E}}(s) - \Delta P_{\mathrm{L}}(s)}{2Hs + D} \tag{6}$$

where H denotes the equivalent inertia time constant of the system, D denotes the load damping coefficient, and $\Delta P_{\mathrm{L}}(s)$ denotes the power increment caused by the load disturbance.

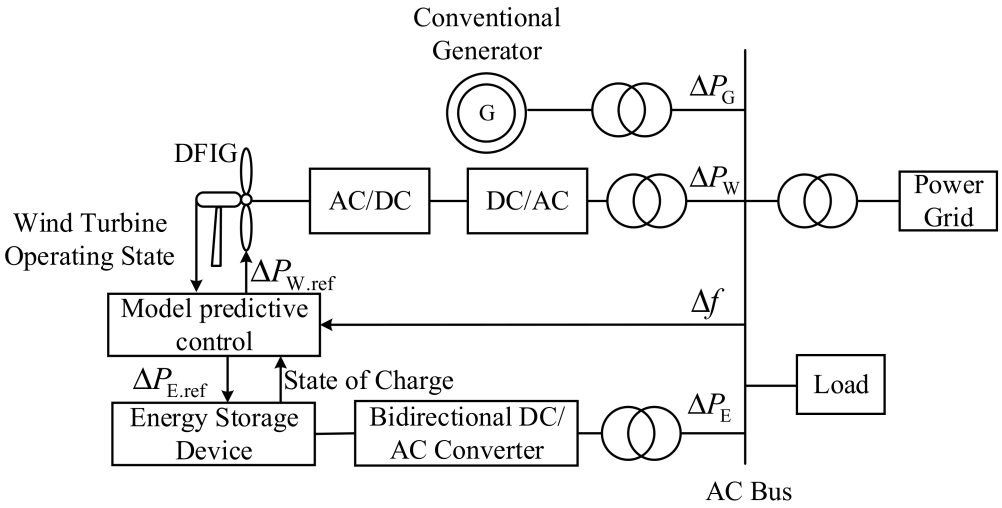


Figure 1. Structure of the wind-storage coordinated system.

The primary frequency regulation characteristics of the conventional synchronous generating unit can be described by the governor–turbine model, and its transfer function can be expressed as:

$$\Delta P_{\mathrm{G}}(s) = G_{\mathrm{gov}}(s)G_{\mathrm{gen}}(s)\left[-\frac{1}{R_{\mathrm{G}}}\Delta f(s)\right] \tag{7}$$

where $G_{\mathrm{gov}}(s)$ and $G_{\mathrm{gen}}(s)$ denote the transfer functions of the governor and the turbine, respectively, and R_{G} denotes the droop coefficient adopted by the conventional synchronous generating unit in primary frequency regulation.

For the purpose of system-level primary frequency regulation analysis on the electromechanical time scale, the wind turbine active-power response is represented in this study by an equivalent reduced-order model combining synthetic inertia and droop support. Rather than reproducing detailed converter-interfaced electromagnetic transients, this representation is intended to capture the dominant frequency-support behavior relevant to upper-layer coordinated control. Accordingly, the wind turbine frequency response transfer function can be written in the following equivalent form:

$$\Delta P_{\mathrm{W}}(s) = \frac{K_{\mathrm{b}}s + K_{\mathrm{p}}}{T_{\mathrm{W}}s + 1}\Delta f(s) \tag{8}$$

where K_{b} denotes the virtual inertia control coefficient of the wind turbine, K_{p} denotes the virtual droop control coefficient, and T_{W} denotes the equivalent response time constant of the wind turbine.

Similarly, on the same electromechanical frequency-regulation time scale, the supercapacitor energy storage unit is represented by an equivalent reduced-order active-power response model under virtual droop control. This formulation is adopted to describe the dominant power-support dynamics required for coordinated frequency-response-oriented

analysis, while detailed converter-level transients are beyond the modeling scope of the present study. Accordingly, its transfer function can be expressed as:

$$\Delta P_{\mathrm{E}}(s) = \frac{K_{\mathrm{E}}}{T_{\mathrm{E}}s + 1}\Delta f(s) \tag{9}$$

where K_{E} denotes the virtual droop control coefficient of the energy storage unit, and T_{E} denotes the equivalent response time constant of the energy storage unit.

By further combining the above components, the overall hierarchical coordinated control framework together with the equivalent frequency response model of the wind–storage hybrid system can be obtained, as shown in Figure 2.

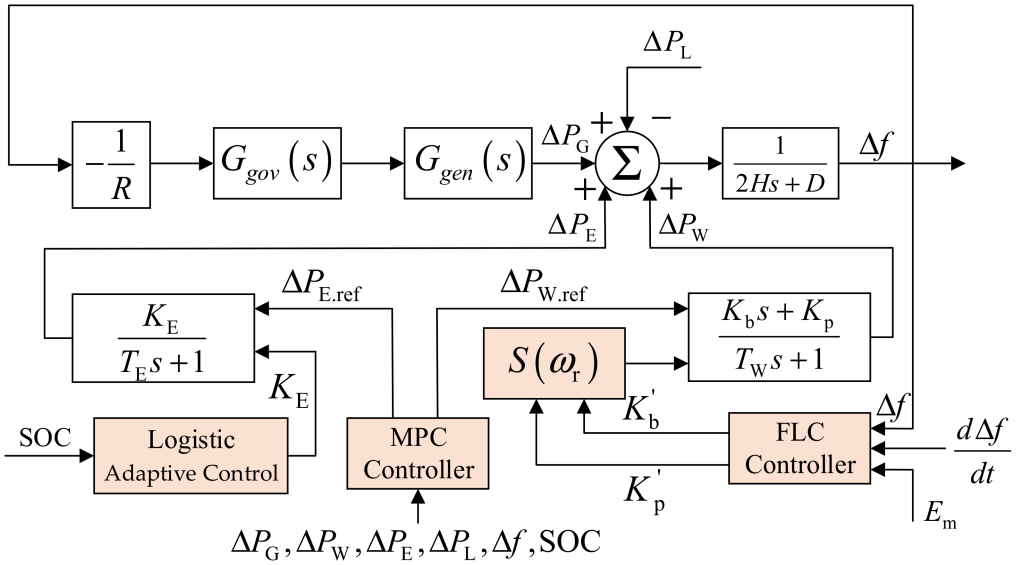


Figure 2. Overall hierarchical coordinated control framework and equivalent frequency response model of the wind–storage hybrid system.

As shown in Figure 2, the proposed strategy adopts a hierarchical coordinated control structure composed of a local adaptive control layer and an upper-layer MPC coordinator. At the local control layer, the wind turbine support capability is determined by the multivariable fuzzy logic controller and the rotor-speed safety attenuation mechanism, whereas the storage-side support capability is adjusted by the SOC-dependent adaptive droop law. On this basis, the MPC serves as the upper-layer coordinator to update the reference power commands of the wind turbine and the energy storage unit in a rolling manner according to the predicted system states and frequency response. In this way, the local controllers provide state-dependent fast support, while the upper layer coordinates the power allocation between the two units.

In this study, several reduced-order modeling assumptions are adopted to focus on the system-level primary frequency regulation mechanism of the wind–storage hybrid system on the electromechanical time scale. Accordingly, the converter-related active-power responses of the wind turbine and the energy storage unit are represented by equivalent first-order links with corresponding time constants, the communication process between the upper-layer coordinator and the local controllers is assumed to be ideal, and the supercapacitor is described by an equivalent RC-based model. Under this framework, the upper-layer MPC is formulated on the basis of a reduced-order prediction model for frequency-response-oriented coordinated power allocation, rather than for detailed converter-level EMT or RMS transient reproduction. Therefore, the conclusions of the present work should be interpreted within the scope of electromechanical time-scale pri-

mary frequency regulation analysis, while the influence of higher-fidelity device dynamics and communication imperfections will be further investigated in future work.

2.2. State-Aware Coordinated Frequency Regulation Strategy for the Wind–Storage Hybrid System

2.2.1. Coordinated Frequency Regulation Strategy for the Wind–Storage Hybrid System Under Multiple Wind Speed Regions

The DFIG is connected to the grid through a back-to-back converter, by which the rotor speed is decoupled from the grid frequency. To enable the wind turbine to participate in frequency regulation, a synthetic inertia control scheme is introduced in this paper, such that the turbine provides additional active power associated with the system frequency rate of change df/dt and the frequency deviation Δf. The corresponding response equation can be expressed as:

$$\Delta P_{\mathrm{W}} = K_{\mathrm{b}} \frac{d\Delta f}{dt} + K_{\mathrm{p}} \Delta f \tag{10}$$

The frequency regulation capability of a wind turbine is inherently limited by its available rotor kinetic energy reserve, rotor-speed safety margin, and remaining active power regulation margin under the current operating condition. Accordingly, the wind speed is classified in this paper into three operating regions, and the corresponding wind–storage coordinated frequency regulation roles are assigned according to the effective and safe regulation capability available in each region.

Low wind speed region: In this region, the rotor speed remains close to the minimum grid-connection threshold, and the available kinetic energy reserve is insufficient. If rotor kinetic energy is further extracted for frequency support, the rotor speed may readily decrease below the safety limit, which can lead to cascading disconnection of the unit. Therefore, the wind turbine is excluded from primary frequency regulation in this region, and the energy storage system, owing to its fast response capability, is solely responsible for providing frequency support.

Medium wind speed region: In this region, the wind turbine operates under MPPT conditions and possesses sufficient rotor kinetic energy reserve together with adequate converter margin, thereby offering the most favorable operating condition for frequency regulation. Under this circumstance, the wind turbine acts as the major frequency support source and adopts synthetic inertia control, while the energy storage system provides supplementary support in a coordinated manner according to the turbine operating state so as to jointly mitigate frequency fluctuations.

High wind speed region: In this region, the wind turbine approaches rated full-power operation, and both the rotor speed and active power output become close to their physical limits. As a result, the available rotor kinetic energy margin is extremely restricted, and forced participation in frequency regulation may cause equipment overload or control instability. Accordingly, the wind turbine is also prevented from participating in frequency regulation in this region, and the energy storage system assumes the principal role in frequency support instead.

Based on the above analysis, the energy storage system is mainly employed to reduce the steady-state frequency deviation and compensate for the power shortfall of the wind turbine. Hence, virtual droop control is adopted, and the corresponding output power can be expressed as:

$$\Delta P_{\mathrm{E}} = -K_{\mathrm{E}} \Delta f \tag{11}$$

2.2.2. Multivariable Fuzzy Synthetic Inertia Control of Wind Turbines Considering Rotor Speed Constraints

In the medium wind speed region, when the wind turbine releases kinetic energy to participate in frequency regulation, the rotor speed must be strictly constrained within the

safe operating range to prevent the turbine from disconnecting from the grid due to stall or overspeed. According to the safe operating characteristics of the doubly fed induction generator, the safe rotor speed range is set to 0.7~1.2 p.u. in this paper. To evaluate the frequency regulation potential of the wind turbine, the available rotor kinetic energy margin is introduced, which can be expressed as:

$$E_{\mathrm{m}} = \begin{cases} \frac{\omega_{\mathrm{r}}^2 - \omega_{\mathrm{min}}^2}{\omega_{\mathrm{opt}}^2 - \omega_{\mathrm{min}}^2}, \Delta f < 0 \\ \frac{\omega_{\mathrm{max}}^2 - \omega_{\mathrm{r}}^2}{\omega_{\mathrm{max}}^2 - \omega_{\mathrm{opt}}^2}, \Delta f > 0 \end{cases} \tag{12}$$

where ω_{opt} is the optimal reference rotor speed under MPPT operation, and $E_{\mathrm{m}} \in [0,\ 1]$ is the available energy margin, which dynamically characterizes the energy reserve that can be used for frequency support.

When the unit operates close to ω_{opt}, $E_{\mathrm{m}} \approx 1$, which indicates sufficient kinetic energy reserve. As the rotor speed approaches the safety boundary, $E_{\mathrm{m}} \approx 0$, in which case the unit loses its frequency regulation capability.

Under the medium wind speed operating condition, different frequency regulation capabilities of the wind turbine can be achieved by adjusting the relevant control coefficients. However, it is difficult for the wind turbine to determine its output level directly from real-time operating states. To address this highly uncertain, nonlinear, and multi-objective coordinated control process, FLC provides an effective solution with flexible dynamic response and strong robustness, without relying on an accurate mathematical model [20].

Taking advantage of the fact that FLC does not require an explicit mathematical relationship among variables, a multivariable fuzzy logic controller is constructed in this paper. The available kinetic energy margin E_{m}, rate of change in frequency df/dt, and frequency deviation Δf are selected as the input variables, while the initial virtual inertia coefficient K_{b}' and the initial virtual droop coefficient K_{p}' are taken as the output variables.

For a typical frequency drop condition, the available kinetic energy margin, the rate of change in frequency, and the frequency deviation are respectively defined within [0, 1], $[-0.6,\ 0]$ Hz/s, and $[-1,\ 0]$ Hz. Meanwhile, both the virtual inertia coefficient and the virtual droop coefficient vary within [5, 20]. To construct the fuzzy controller, five linguistic subsets are assigned to both the input and output variables, namely VL, L, M, S, and VS, which represent very large, large, medium, small, and very small, respectively. Their membership functions are illustrated in Figure 3.

The universes of discourse of E_{m}, df/dt, and Δf were determined according to the typical operating range of the studied system under the considered frequency-drop scenarios and preliminary simulation tests. The output ranges of K_{b}' and K_{p}' were selected as [5, 20] to provide sufficient transient support capability while keeping the initial coefficient tuning within a reasonable range under different operating conditions. In addition, five linguistic subsets were adopted as a compromise between control sensitivity and rule-base complexity. The final membership distribution and rule base were further refined through repeated simulation tests to obtain a satisfactory compromise among response speed, support strength, and rotor-speed safety.

In this study, a Mamdani-type fuzzy inference structure is adopted for the wind-turbine-side controller, with the min operator used for fuzzy implication and the max operator used for aggregation. The output variables K_{b}' and K_{p}' are obtained by centroid defuzzification. Since the universes of discourse of all input and output variables are explicitly predefined according to the expected operating range of the studied system, the normalization and scaling processes are embedded in the selected variable ranges and membership mappings, rather than introduced as additional independent gain blocks. The complete fuzzy rule base used to generate K_{b}' and K_{p}' is listed in Appendix A.

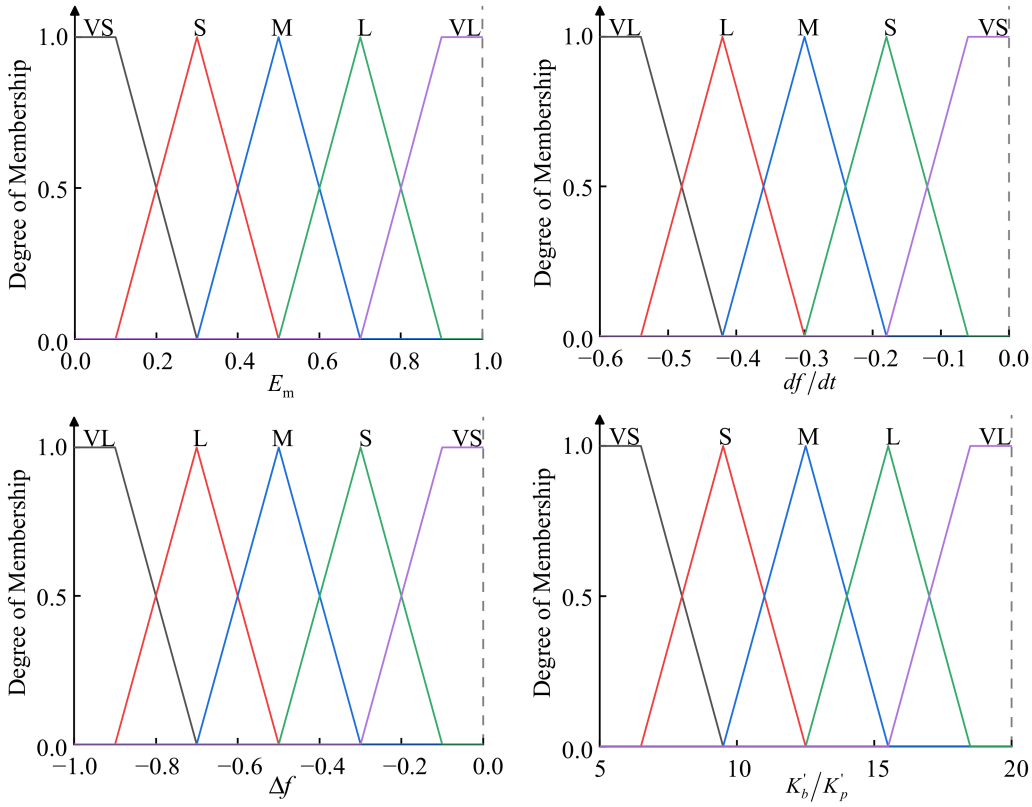


Figure 3. Membership relation curve of input/output variables.

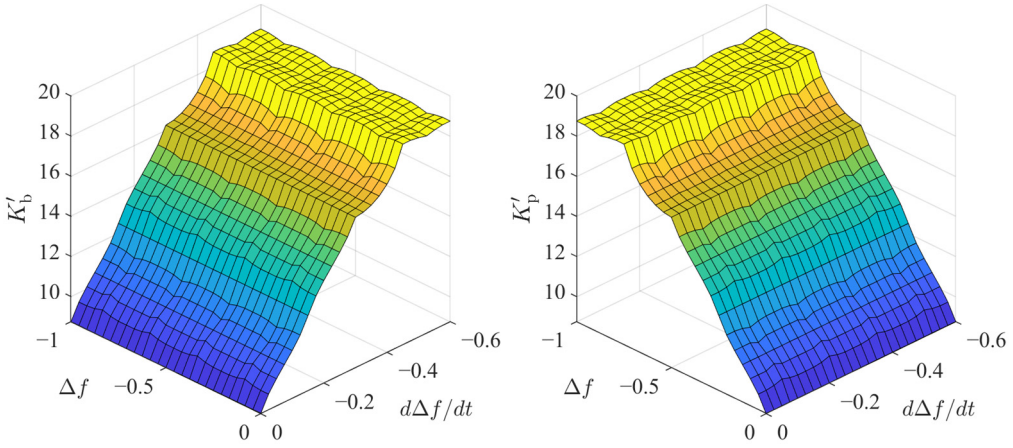
The fuzzy controller proposed in this paper is constructed to reconcile turbine operating safety with the need for system frequency support. Its basic design philosophy is to release the available rotor kinetic energy as much as possible to provide rapid frequency response to the grid while ensuring stable wind turbine operation. The associated fuzzy control rules are given as follows:

Initial stage of frequency decline: At this stage, a sudden power deficit causes the grid frequency to drop rapidly. The absolute value of the rate of change in frequency, $|df/dt|$, is relatively large, whereas the absolute value of the frequency deviation, $|\Delta f|$, remains relatively small. Under this condition, the virtual inertia response of the wind turbine plays a dominant role. If the available kinetic energy margin E_m is at a relatively high level, it indicates that the rotor speed is close to the synchronous speed or in the super synchronous operating state, and that the kinetic energy reserve is sufficient. In this case, the controller outputs a relatively large initial virtual inertia coefficient K_b' and a relatively small initial virtual droop coefficient K_p', so that rotor kinetic energy can be released rapidly within a short time to provide strong transient inertial support for the grid. In contrast, when E_m is low, the rotor speed is already close to the lower safety limit and the frequency regulation potential is severely limited. Under such circumstances, the controller gives priority to the grid-connected stability of the turbine and constrains K_b' to a relatively low level, thereby suppressing the initial power release and avoiding turbine disconnection caused by excessive depletion of rotor kinetic energy.

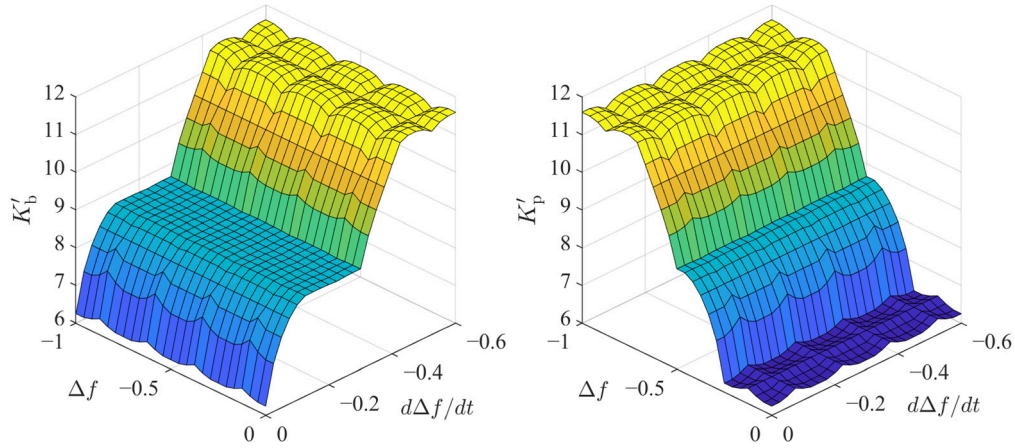
Middle and later stages of frequency decline: As the primary frequency regulation process proceeds, the rate of frequency decline gradually slows down, $|df/dt|$ decreases progressively, while $|\Delta f|$ continues to increase in magnitude and approaches its maximum deviation. At this stage, the virtual droop response of the wind turbine becomes dominant, and K_p' should be gradually increased with the increase in $|\Delta f|$ to compensate for the power deficit. Meanwhile, K_b' should rapidly converge as $|df/dt|$ decreases. If the available kinetic energy margin E_m

drops sharply during this discharge stage, maintaining high-intensity power support would easily break the rotor energy balance. Therefore, when E_m becomes small, the controller limits K'_p to a relatively low level, prompting the wind turbine to actively reduce its output, while the subsequent frequency support is transferred to the energy storage system.

Through the logical inference of the above fuzzy rules, the controller can output the initial synthetic inertia coefficients K'_b and K'_p of the wind turbine in real time. When the available kinetic energy margin E_m is set to 0.8 and 0.2, respectively, the three-dimensional relationship of the initial synthetic inertia coefficients is shown in Figure 4.



(**a**) Initial Frequency Regulation Coefficients at an Energy Margin of 0.8



(**b**) Initial Frequency Regulation Coefficients at an Energy Margin of 0.2

Figure 4. Fuzzy logic inference result of fan comprehensive inertia coefficient.

The coefficients K'_b and K'_p obtained through fuzzy logic inference represent the expected coefficient values under ideal conditions. However, under extreme grid load disturbances, even if the fuzzy controller reduces the frequency regulation coefficients to their minimum values, sustained active power output may still cause the wind turbine to disconnect from the grid due to excessive response. To compensate for the limitations of FLC under extreme operating conditions, a nonlinear safety attenuation function $S(\omega_r)$ is introduced in this paper to dynamically modify the boundaries of the initial frequency regulation coefficients, as given by:

$$S(\omega_r) = \begin{cases} 1 - e^{-\mu(\omega_r - \omega_{min})}, \Delta f < 0 \\ 1 - e^{-\mu(\omega_{max} - \omega_r)}, \Delta f > 0 \end{cases} \quad (13)$$

where μ denotes the penalty adjustment coefficient, which is used to characterize the sensitivity and smoothness of the turbine when withdrawing from frequency regulation.

The parameter μ governs the sensitivity and smoothness of the attenuation process when the rotor speed approaches the safety boundary. A relatively small μ leads to overly early attenuation and may weaken the transient frequency support capability of the wind turbine, whereas an excessively large μ makes the attenuation too slow to effectively restrain further rotor-speed decline near the safety limit. Therefore, $\mu = 30$ is selected in this study as a compromise between rotor kinetic energy utilization and rotor-speed protection under the considered operating conditions. The attenuation function curve during a frequency drop event under this parameter setting is shown in Figure 5.

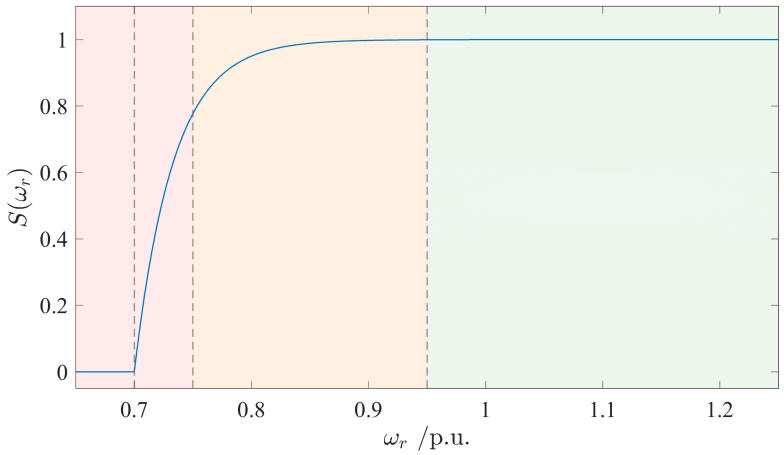


Figure 5. Curve of the Nonlinear Safety Attenuation Function.

As shown in Figure 5, the nonlinear attenuation mechanism divides the wind turbine operation into three dynamic response regions:

Normal operating region ($\omega_r > 0.95$ p.u.): In this region, the rotor speed has sufficient margin, and the available kinetic energy is abundant. The attenuation function, therefore, introduces almost no intervention, i.e., $S(\omega_r) \approx 1$, which ensures the maximum release of the wind turbine's frequency regulation potential.

Smooth warning region ($0.75 < \omega_r < 0.95$ p.u.): As the rotor speed decreases, the available kinetic energy margin is gradually reduced. When the rotor speed drops to the warning boundary of 0.75 p.u., the attenuation function decreases to 0.777, and the system starts to forcibly restrain the frequency regulation output of the wind turbine so as to prevent the rotor kinetic energy from being depleted too rapidly.

Safety blocking region ($\omega_r < 0.75$ p.u.): When the rotor speed approaches the minimum safety limit of 0.7 p.u., the attenuation function decays exponentially to zero.

Accordingly, the variable-coefficient tuning formula of the synthetic inertia control for the wind turbine can be written as:

$$K_b = K'_b \cdot S(\omega_r) \tag{14}$$

$$K_p = K'_p \cdot S(\omega_r) \tag{15}$$

Since the attenuation function satisfies $0 \leq S(\omega_r) \leq 1$ within the admissible rotor-speed range, the actual coefficients always satisfy $0 \leq K_b \leq K'_b$ and $0 \leq K_p \leq K'_p$. Therefore, the proposed attenuation mechanism does not amplify the initial fuzzy control outputs, but only provides a bounded safety correction when the rotor speed approaches its lower operating boundary.

2.2.3. Adaptive Droop Control of Energy Storage Considering Asymmetric SOC Constraints

To maintain the SOC of the energy storage system within a reasonable range, its regulation gain should be properly designed. Conventional virtual droop control generally

employs a fixed droop coefficient; that is, the maximum coefficient is continuously applied in response to frequency deviation regardless of the SOC level [21]. This strategy can effectively suppress frequency fluctuations when the SOC is sufficient. However, when the SOC approaches the lower safety limit, continuous output at the maximum power level will lead to rapid depletion of the storage capacity. This not only weakens the subsequent frequency regulation capability of the system but may also cause secondary disturbances during grid frequency recovery due to the premature withdrawal of the energy storage unit from operation. Owing to its monotonicity and convex–concave characteristics, the Logistic function naturally satisfies the requirement that the droop coefficient should vary adaptively with SOC. On this basis, an adaptive control strategy for energy storage based on the Logistic function is proposed in this paper so that the output of the storage unit can be adjusted in real time during frequency regulation [22]. The SOC is divided into different regions, where 0.1, 0.45, 0.55, and 0.9 are defined as the minimum, relatively low, relatively high, and maximum SOC values, respectively. The corresponding expression can be written as [23]:

$$K_c = \begin{cases} K_{max}, \mathrm{SOC} \in (0, 0.1] \\ \dfrac{K_{max} P_0 \cdot e^{\frac{n \cdot (0.9 - \mathrm{SOC})}{0.35}}}{K_{max} + P_0 \cdot \left(e^{\frac{n \cdot (0.9 - \mathrm{SOC})}{0.35}} - 1 \right)}, \mathrm{SOC} \in (0.1, 0.9] \\ 0, \mathrm{SOC} \in (0.9, 1] \end{cases} \tag{16}$$

$$K_d = \begin{cases} 0, \mathrm{SOC} \in (0, 0.1] \\ \dfrac{K_{max} P_0 \cdot e^{\frac{n \cdot (\mathrm{SOC} - 0.1)}{0.35}}}{K_{max} + P_0 \cdot \left(e^{\frac{n \cdot (\mathrm{SOC} - 0.1)}{0.35}} - 1 \right)}, \mathrm{SOC} \in (0.1, 0.9] \\ K_{max}, \mathrm{SOC} \in (0.9, 1] \end{cases} \tag{17}$$

where K_c is the charging control coefficient; K_d is the discharging control coefficient; K_{max} is the maximum value of the virtual unit regulation power; p_0 and n are the adaptive factors of the curve, which can influence the trend and shape of the curve. The curves corresponding to p_0 and n under different parameter values are shown in Figures 6 and 7, respectively.

To ensure that the SOC of the energy storage system remains within its prescribed limits while also taking the response speed of the storage system into account, $p_0 = 0.01$ and $n = 20$ are selected in this paper. The resulting KE-SOC curve is shown in Figure 8.

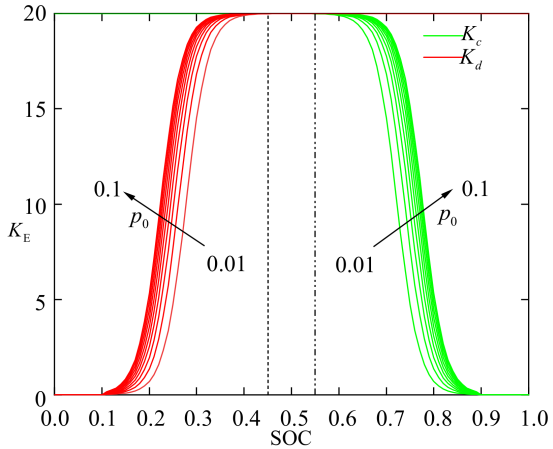


Figure 6. Change curve of stored energy SOC with p_0.

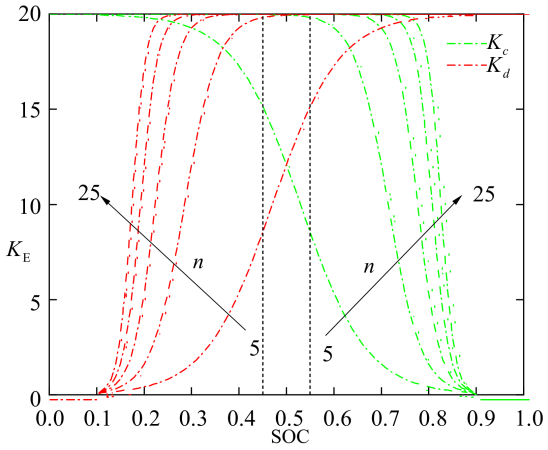


Figure 7. Change curve of stored energy SOC with n.

It should be noted that the zero-coefficient segments in (16) and (17) are introduced as protective blocking regions rather than ordinary regulation regions. Specifically, when the SOC falls into the lower protection interval, the discharging-side droop action is blocked to prevent further over-discharge; similarly, when the SOC enters the upper protection interval, the charging-side droop action is blocked to avoid over-charge. Owing to the adopted Logistic-function-based design, the corresponding droop coefficient already approaches its limiting value smoothly before reaching the protection boundary. In particular, with $p_0 = 0.01$, the coefficient is already very close to zero near the blocking boundary, so the transition to the zero-coefficient protection state does not introduce an obvious discontinuity in the control signal. In addition, the actual storage power response is still filtered by the equivalent first-order dynamic link, while the remaining frequency support demand is coordinated by the wind turbine, conventional units, and the upper-layer MPC framework. Therefore, the proposed protection mechanism mainly acts as a smooth directional withdrawal of storage support, rather than an abrupt destabilizing switching action.

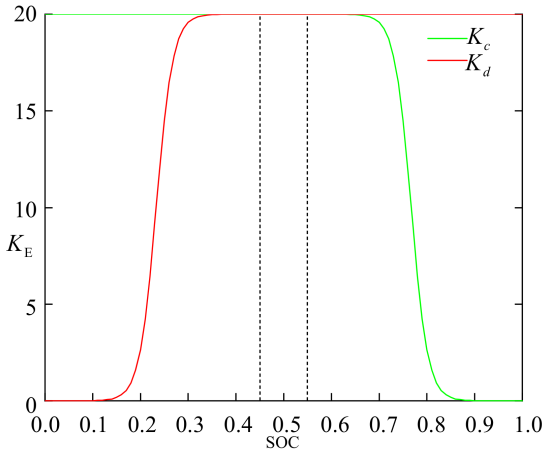


Figure 8. Adaptive change trend of energy storage SOC.

2.3. Coordinated Output Power Optimization of the Wind–Storage Hybrid System Based on MPC

2.3.1. Establishment of the Predictive Control Model

In this study, the MPC is employed as an upper-layer coordinator to generate rolling reference power commands for the wind turbine and the energy storage unit on the basis of the local control laws described in Section 2.2.

As can be seen from Figure 1, the set of equations of the wind–storage hybrid system during the primary frequency regulation process can be expressed as:

$$\begin{cases} \Delta P_{\mathrm{G}} = -\frac{1}{R} G_{\mathrm{gov}}(s) G_{\mathrm{gen}}(s) \Delta f \\ \Delta P_{\mathrm{W}} = \Delta P_{\mathrm{W.ref}} G_{\mathrm{W}}(s) \\ \Delta P_{\mathrm{E}} = \Delta P_{\mathrm{E.ref}} G_{\mathrm{E}}(s) \\ \Delta f = (\Delta P_{\mathrm{G}} + \Delta P_{\mathrm{W}} + \Delta P_{\mathrm{E}} - \Delta P_{\mathrm{L}}) \frac{1}{2Hs+D} \end{cases} \tag{18}$$

For the energy storage unit, the state of charge varies dynamically during the charging and discharging process. Neglecting the effect of charging/discharging efficiency, the SOC can be expressed as:

$$\Delta S_{\mathrm{soc}} = S_{\mathrm{soc}} - \Delta P_{\mathrm{E}} T / E_{\mathrm{s}} \tag{19}$$

where S_{soc} denotes the state of charge of the energy storage unit, T denotes the sampling interval in the predictive control model, and E_{s} denotes the rated capacity of the energy storage system.

For the system under study, the linearized prediction model in standard form can be written as:

$$\begin{cases} x(k+1) = Ax(k) + B\Delta u(k) + Rr(k) \\ y(k) = Cx(k) \end{cases} \tag{20}$$

where k denotes the current sampling instant; x and y denote the system state variable and output variable, respectively; Δu and r denote the control input and disturbance variable, respectively; and A, B, C, R denote the state matrix, control input matrix, output matrix, and external disturbance matrix, respectively.

By discretizing (20) in accordance with the standard form of (18), the resulting discrete-time equation can be obtained as:

$$\begin{cases} \Delta P_{\mathrm{G}}(k+1) = \left(1 - \frac{T}{T_{\mathrm{G}}}\right) \Delta P_{\mathrm{G}}(k) + \frac{T}{T_{\mathrm{G}}} \Delta f(k) \\ \Delta P_{\mathrm{W}}(k+1) = \left(1 - \frac{T}{T_{\mathrm{W}}}\right) \Delta P_{\mathrm{W}}(k) + \frac{T}{T_{\mathrm{W}}} \Delta P_{\mathrm{W.ref}} \\ \Delta P_{\mathrm{E}}(k+1) = \left(1 - \frac{T}{T_{\mathrm{E}}}\right) \Delta P_{\mathrm{E}}(k) + \frac{T}{T_{\mathrm{E}}} \Delta P_{\mathrm{E.ref}} \\ S(k+1) = S(k) - \Delta P_{\mathrm{E}}(k) \frac{T}{E_{\mathrm{s}}} \\ \Delta f(k+1) = \left(1 - \frac{DT}{2H}\right) \Delta f(k) + \frac{T}{2H} [\Delta P_{\mathrm{G}}(k) + \Delta P_{\mathrm{W}}(k) + \Delta P_{\mathrm{E}}(k) - \Delta P_{\mathrm{L}}(k)] \end{cases} \tag{21}$$

The state variable vector in this model is:

$$x(k) = [\Delta P_{\mathrm{G}}(k), \Delta P_{\mathrm{W}}(k), \Delta P_{\mathrm{E}}(k), S(k), \Delta f(k)]^T \tag{22}$$

The output variable vector is:

$$y(k) = [\Delta P_{\mathrm{W}}(k), \Delta P_{\mathrm{E}}(k), S(k), \Delta f(k)]^T \tag{23}$$

The disturbance variable vector is:

$$r(k) = \Delta P_{\mathrm{L}}(k) \tag{24}$$

2.3.2. Objective Function

To achieve the coordinated optimal allocation of the reference power commands of the wind turbine and the energy storage unit during the primary frequency regulation process of

the wind–storage hybrid system, while simultaneously taking the system frequency regulation performance into account, the following objective function is constructed in this paper:

$$J_{\min} = \alpha \sum_{i=1}^{N_p} \Delta f^2(k+i|k) - f(k+i) + \beta \sum_{i=0}^{N_c} \Delta P_{W.ref}^2(k+i|k) + \gamma \sum_{i=0}^{N_c} \Delta P_{E.ref}^2(k+i|k)^2 \quad (25)$$

where $\Delta f(k+i|k)$ denotes the predicted value of the system frequency deviation Δf at time $k+i$ based on the information available at time k; $\Delta P_{W.ref}(k+i|k)$ and $\Delta P_{E.ref}(k+i|k)$ denote the reference control increments of the wind turbine and the energy storage unit, respectively.

The objective function in (25) consists of three parts. The first term penalizes the predicted system frequency deviation over the prediction horizon, so as to improve the frequency support performance of the wind–storage hybrid system. The second and third terms penalize the increments of the wind turbine reference power and the energy storage reference power over the control horizon, respectively, thereby avoiding excessive command variation and improving the smoothness of coordinated power allocation. Therefore, the objective function represents a compromise between frequency regulation effectiveness and control-action smoothness.

In the present study, the weighting coefficients α, β, and γ are treated as preset tuning parameters rather than dynamically updated variables. Among them, α is assigned a relatively large value to emphasize the suppression of frequency deviation, whereas β and γ are assigned relatively smaller values to limit overly aggressive output adjustments of the wind turbine and the energy storage unit. In this way, the selected weighting coefficients reflect the desired balance among frequency support performance, coordinated wind–storage participation, and control smoothness under the studied operating conditions. In addition, the prediction horizon $N_p = 20$ and the control horizon $N_c = 19$ were selected by considering the dominant time scale of primary frequency regulation together with the computational burden of receding-horizon optimization.

2.3.3. Constraints

(1) Constraint on the active power increment of the wind turbine

To avoid severe fluctuations in the wind turbine reference power between adjacent control instants, the increment of the wind turbine power command is constrained as:

$$-\Delta P_{W.max} \le \Delta P_{W.ref}(k+i|k) \le \Delta P_{W.max} \quad (26)$$

where $\Delta P_{W.max}$ denotes the maximum active power increment of the wind turbine.

(2) Output constraint of the energy storage unit

During the charging and discharging process, the output of the energy storage unit is limited by its rated power. The corresponding constraint can be expressed as:

$$-P_{E.N} \le \Delta P_{E.ref}(k+i|k) \le P_{E.N} \quad (27)$$

where $P_{E.N}$ denotes the rated power of the energy storage unit.

(3) SOC constraint of the energy storage unit

The SOC of the energy storage unit should remain within its allowable operating limits. The constraint condition is given by:

$$S_{soc.min} \le S_{soc}(k+i|k) \le S_{soc.max} \quad (28)$$

where is the predicted value at time for at time.

(4) Frequency balance constraint for primary frequency regulation

According to general standards, the absolute value of the steady-state frequency deviation after completion of primary frequency regulation should not exceed 0.2 Hz [24,25]. If the load fluctuation is small and the primary frequency regulation task can be accomplished solely by conventional generating units, the system output reaches its maximum value when the system attains the steady state:

$$\Delta P_{\mathrm{G.max}} = (-1/R - D)\Delta f_{\mathrm{ref}} \tag{29}$$

where $\Delta f_{\mathrm{ref}} = \pm 0.2$ Hz.

When the system output is optimized by the rolling optimization of MPC, if $|P_{\mathrm{L}}(k+i|k)| \leq |\Delta P_{\mathrm{G.max}}|$, the participation of the wind–storage system in frequency regulation is not required. Here, $|P_{\mathrm{L}}(k+i|k)|$ denotes the absolute value of the predicted P_{L} at time $k+i$ based on the information available at time k. If $|P_{\mathrm{L}}(k+i|k)| > |\Delta P_{\mathrm{G.max}}|$, the wind–storage hybrid system is required to participate in frequency regulation. In this case, the wind–storage hybrid system and the power grid are regarded as an integrated whole. Let denote the overall primary frequency regulation coefficient of the system. Then,

$$K_i = \frac{P_{\mathrm{L}}(k+i|k)}{\Delta f_{\mathrm{ref}}(k+i|k)} \tag{30}$$

where $\Delta f_{\mathrm{ref}}(k+i|k)$ denotes the prescribed steady-state frequency deviation of the system at time $k+i$ predicted at time k, which is set to ± 0.2 Hz.

The real-time predicted value of the overall system power during the primary frequency regulation process can be expressed as:

$$P(k+i|k) = (K+D)\Delta f(k+i|k) \tag{31}$$

where $P(k+i|k)$ denotes the predicted value of the overall system power demand at time $k+i$ based on the information available at time k.

According to the above analysis, when the wind–storage hybrid system participates in frequency regulation, the overall system power demand should be equal to the sum of the frequency regulation outputs of all components:

$$P(k+i|k) = \Delta P_{\mathrm{G}}(k+i|k) + \Delta P_{\mathrm{W}}(k+i|k) + \Delta P_{\mathrm{E}}(k+i|k) \tag{32}$$

2.3.4. Model Solution

With the prediction model, objective function, and multiple constraints established above, the primary frequency regulation power allocation problem of the wind–storage hybrid system is reformulated as a constrained optimization problem over a receding horizon. During each sampling period, the MPC determines the optimal active power reference trajectories for the wind turbine and the energy storage unit by solving the multivariable constrained problem with the MATLAB/Simulink R2022b (MathWorks, Natick, MA, USA) built-in optimizer, after which the first control input is applied to the lower-level execution layer. By repeatedly updating the optimization in a rolling manner, the wind turbine and the energy storage unit are coordinated more effectively across different response times and regulation characteristics. The resulting complementary operation can be interpreted in the following two stages.

Power compensation stage during frequency support: During primary frequency regulation, when the system operates in the low wind speed region or when the wind turbine actively reduces its output because the rotor speed approaches the lower safety limit, conventional local control may result in an abrupt decrease in the overall frequency

regulation power. By contrast, MPC can perceive the output trend of the wind turbine in advance through forward-rolling prediction. Once the optimizer detects that the turbine output has reached the safety constraint boundary and can no longer be further increased, the optimization direction of the power deficit is automatically shifted to the energy storage system, provided that the overall power balance requirement of the system is satisfied. In this manner, the MPC naturally dispatches the energy storage unit to provide rapid power compensation, thereby filling the temporary gap in turbine frequency support.

Coordinated recovery stage during frequency restoration: When the system frequency passes the nadir and gradually recovers toward the steady state, the grid demand for active power support decreases progressively. During this stage, the wind turbine absorbs power from the grid to restore its rotor speed, whereas the energy storage unit may still be delivering power, which gives rise to internal power competition between the two units. By predicting the frequency recovery trajectory in advance, the MPC coordinates the reference outputs of the wind turbine and the energy storage unit in a unified manner, actively suppresses the reverse power absorption behavior of the wind turbine, and smoothly adjusts the droop support strength of the energy storage unit. As a result, the risk of a secondary frequency dip can be effectively avoided.

The MPC-based optimal power allocation framework for frequency regulation of the wind–storage hybrid system is depicted in Figure 9. By means of coordinated optimization, this framework ensures that the system frequency deviation is effectively restrained while further enhancing the complementary regulation potential of the wind turbine and the energy storage unit.

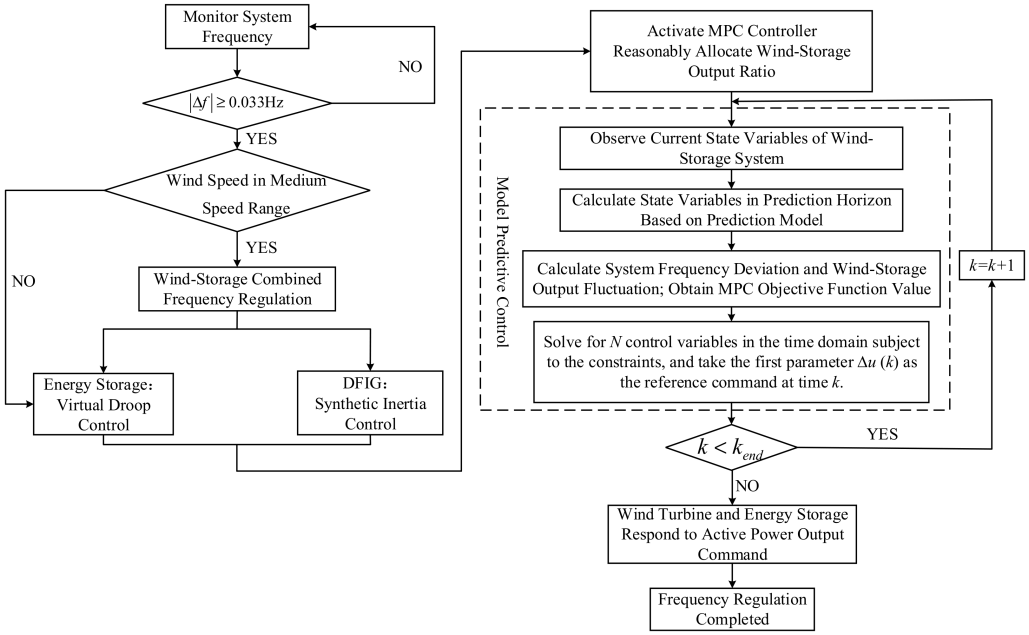


Figure 9. Block diagram of MPC-based frequency regulation power optimal allocation for a wind-storage combined system.

2.3.5. Remarks on Closed-Loop Stability

From the perspective of control structure, the proposed method adopts a hierarchical framework composed of bounded local adaptive control laws and an upper-layer MPC-based power allocation mechanism. Under the adopted frequency response model, the wind turbine branch and the energy storage branch are represented by first-order equivalent dynamic links with positive time constants, as shown in (8) and (9). Therefore, when the control coefficients remain within their admissible ranges, the corresponding local response dynamics are bounded.

For the wind turbine branch, the multivariable fuzzy logic controller generates the initial coefficients K'_b and K'_p within predefined finite intervals. These initial coefficients are further corrected by the nonlinear safety attenuation function $S(\omega_r)$, so that the actual coefficients K_b and K_p remain bounded during the frequency regulation process. In this way, the attenuation mechanism does not introduce unbounded gain variation, but instead restrains the turbine response when the rotor speed approaches the safety boundary.

For the energy storage branch, the adaptive droop coefficient is determined by the Logistic-function-based control law according to the SOC condition. Since the corresponding regulation gain is designed within a finite interval, the storage-side support action is also bounded. Moreover, the storage power and SOC are explicitly restricted by the operating constraints considered in the predictive control model.

At the upper layer, the MPC updates the reference power commands of the wind turbine and the energy storage unit by solving a constrained optimization problem based on the linear prediction model and the imposed power/SOC constraints. Since the decision variables are explicitly bounded, the optimized reference commands remain finite under the studied operating conditions. Accordingly, the proposed coordinated strategy maintains bounded closed-loop responses in the considered disturbance scenarios and exhibits satisfactory dynamic stability in the simulation results.

It should be noted that the present study mainly focuses on mechanism analysis and controller validation under the adopted dynamic model. A rigorous Lyapunov-based proof for the nonlinear fuzzy-attenuation mechanism, or a formal recursive-feasibility and convergence proof for the constrained MPC, is beyond the scope of the present work and will be further investigated in future studies.

3. Results

3.1. Simulation Setup

As shown in Figure 10, a classical four-machine two-area system was established in MATLAB/Simulink R2022b to verify the effectiveness of the proposed coordinated primary frequency regulation strategy for the wind–storage hybrid system.

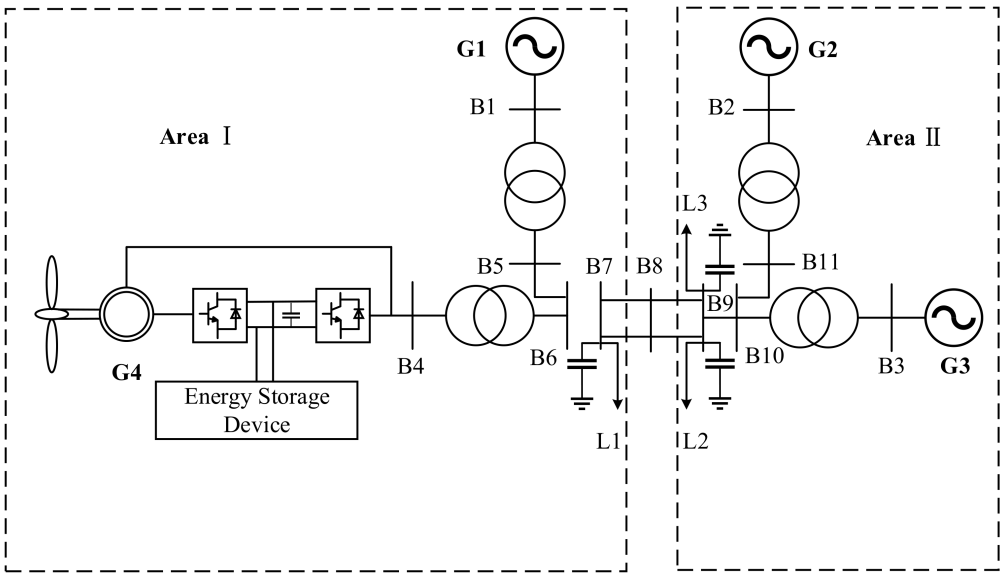


Figure 10. Four-machine two-area simulation model, where Area I and Area II denote the two interconnected areas of the benchmark power system.

In this model, G1–G3 represent thermal power units with a total installed capacity of 300 MW, while G4 represents an aggregated equivalent DFIG-based wind farm composed

of 100 units with an individual rated capacity of 1.5 MW, corresponding to a total installed capacity of 150 MW. This equivalent representation is adopted to facilitate frequency-response-oriented system-level modeling and coordinated control analysis. L1 and L2 are modeled as constant active loads, and L3 is modeled as a randomly fluctuating load. As listed in Table 2, the rated capacity of the energy storage system is 1.2 MW·h, the rated power is 15 MW, the sampling step size is 0.1 s, the prediction horizon is 20, and the control horizon is 19. In addition, all variables are normalized in per-unit values with 100 MW selected as the base value.

Table 2. Main simulation parameters of the wind–storage hybrid system.

Parameters	Value
Sampling step size T/s	0.1
Prediction horizon N_p	20
Control horizon N_c	19
Grid inertia time constant H	4
Load regulation coefficient D	2
Total installed capacity of the wind farm/MW	150
Initial wind speed $v_0/(m/s)$	10
Capacity of the energy storage device $E_s/MW \cdot h$	1.2
Rated power of energy storage $P_{E.N}/MW$	15
Response time of energy storage T_E	0.1
Maximum state of charge S_{max}	0.9
Minimum state of charge S_{min}	0.1
Reference state of charge S_{ref}	0.5

The validation studies in Sections 3.2–3.4 are arranged in a progressive manner. Specifically, Section 3.2 focuses on the benchmark comparison of the wind-turbine-side local control strategy, Section 3.3 examines the storage-side adaptive droop strategy, and Section 3.4 further evaluates the overall coordinated control performance of the complete wind–storage framework. In this way, the proposed method is validated hierarchically from the local control level to the full coordinated control level.

3.2. Validation of the Rotor-Speed-Constrained Synthetic Inertia Control Strategy

As shown in Figure 11, a 0.02 p.u. step load disturbance was introduced at t = 20 s under a constant wind speed of 10 m/s to evaluate the proposed variable-coefficient synthetic inertia control strategy with rotor speed safety constraints. Four cases were compared, including no wind turbine participation in frequency regulation (Strategy 1), fixed-coefficient control (Strategy 2), unconstrained variable-coefficient FLC-based control (Strategy 3), and the proposed constrained variable-coefficient FLC-based strategy (Strategy 4). For clarity, the representative quantitative comparison results of the four strategies are further summarized in Table 3.

As shown in Figure 11b, when the wind turbine did not participate in frequency regulation, the system exhibited the largest frequency deviation, and the frequency nadir reached 49.895 Hz. After fixed-coefficient frequency regulation was introduced, the nadir increased to 49.915 Hz. Under the proposed constrained variable-coefficient FLC strategy, the minimum frequency further improved to 49.924 Hz. In terms of the maximum frequency deviation, the proposed constrained variable-coefficient FLC strategy achieves a reduction of 27.62% compared with the case without wind turbine participation and 10.59% compared with the fixed-coefficient control case. These results indicate that the proposed method can provide more effective transient frequency support under sudden load increase conditions.

As shown in Figure 11c, the maximum additional output power of the wind turbine under fixed-coefficient control is 0.0136 p.u., whereas the proposed variable-coefficient FLC-based strategy increases the peak support power to 0.0169 p.u. This corresponds to

an increase of 24.26%, demonstrating that the proposed strategy can release rotor kinetic energy more effectively during the initial stage of the disturbance and thereby alleviate the system power deficit more rapidly.

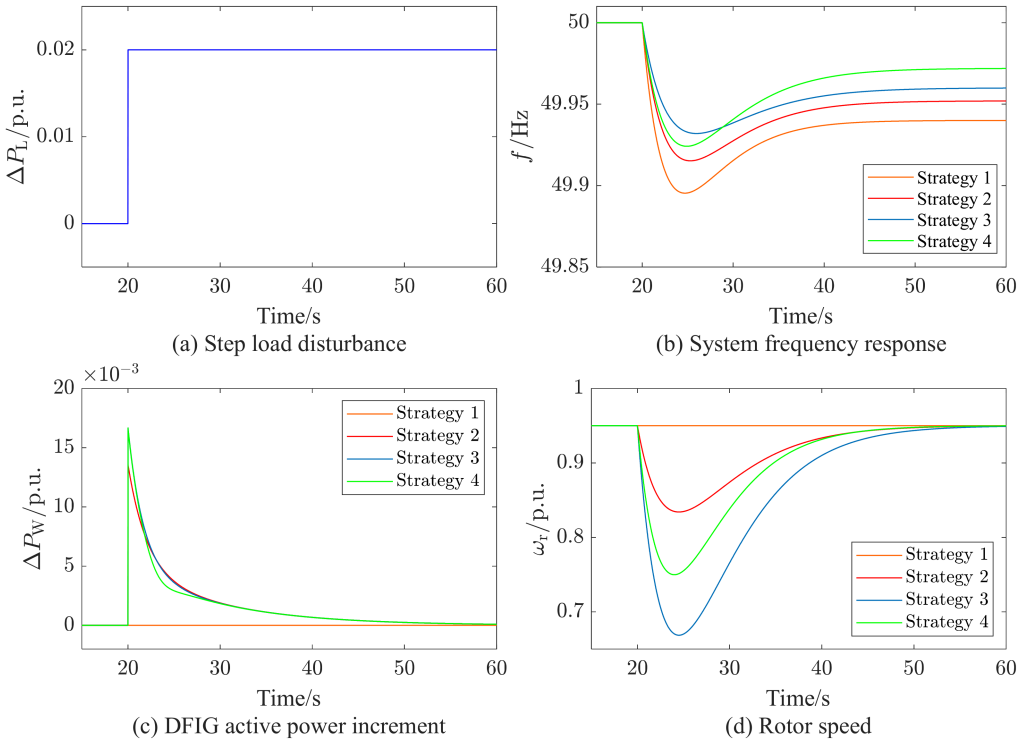


Figure 11. Simulation results of wind turbine under different strategies during a sudden load increase.

Table 3. Quantitative comparison of different wind turbine frequency regulation strategies.

Performance Index	Strategy 1	Strategy 2	Strategy 3	Strategy 4
Maximum frequency deviation Δf_m/Hz	−0.105	−0.085	−0.068	−0.076
Steady-state frequency deviation Δf_s/Hz	−0.061	−0.049	−0.041	−0.029
Maximum additional turbine power $\Delta P_{W.max}$/p.u.	/	0.0136	0.0169	0.0169
Maximum rotor-speed drop $\Delta \omega_r$/p.u.	/	−0.116	−0.281	−0.2

As shown in Figure 11b,d, the unconstrained variable-coefficient FLC can suppress the initial frequency drop more aggressively, but this occurs at the cost of rotor speed violating the safe operating boundary. By contrast, under the proposed constrained strategy, once the rotor speed enters the warning region of 0.75 p.u., the safety constraint is activated and the wind turbine output converges proactively. As a result, the rotor speed remains within the safe operating range, and the steady-state frequency reaches 49.971 Hz. Compared with the unconstrained variable-coefficient FLC case, in which the steady-state frequency is 49.958 Hz, the steady-state frequency error is reduced by 30.95%.

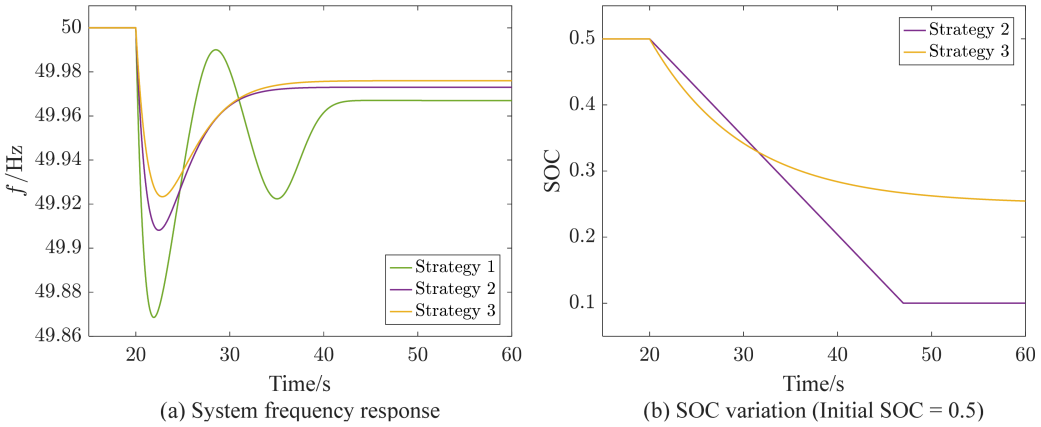
3.3. Validation of the Adaptive Energy Storage Control Strategy

As shown in Table 4 and Figure 12, a 0.02 p.u. step load disturbance was also imposed to verify the proposed adaptive energy storage control strategy under a constant wind speed of 10 m/s. Three cases were examined, namely no energy storage (Strategy 1), energy

storage with fixed-*K* control (Strategy 2), and energy storage with the proposed adaptive control strategy (Strategy 3). The initial SOC of the supercapacitor was set to 0.5, and the simulation duration was 60 s.

Table 4. Evaluation index under different energy storage strategies.

Strategy	The Maximum Frequency Deviation Δf_m/Hz	The Steady-State Frequency Deviation Δf_s/Hz
Strategy 1	−0.131	−0.033
Strategy 2	−0.092	−0.027
Strategy 3	−0.076	−0.024



(a) System frequency response (b) SOC variation (Initial SOC = 0.5)

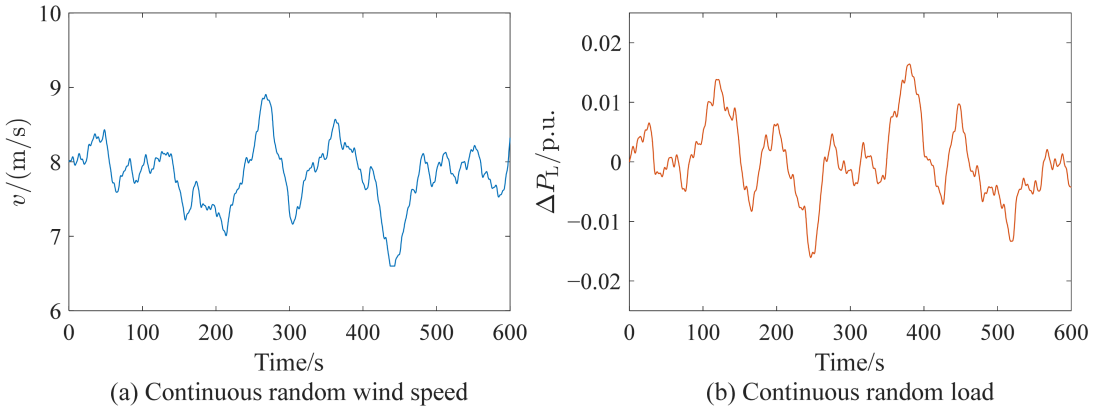
Figure 12. Frequency response under different strategies of energy.

As shown in Table 2 and Figure 12a, when no energy storage was used, the maximum frequency deviation and the steady-state frequency deviation were −0.131 Hz and −0.033 Hz, respectively. After the fixed-*K* method was adopted, these values were reduced to −0.092 Hz and −0.027 Hz. When the proposed adaptive control strategy was applied, the maximum frequency deviation and the steady-state frequency deviation were further reduced to −0.076 Hz and −0.024 Hz, respectively. Compared with the case without energy storage, the proposed strategy improves the maximum frequency deviation by 41.98% and the steady-state frequency deviation by 27.27%. Compared with the non-adaptive energy storage strategy, the corresponding improvements are 17.39% and 11.11%, respectively.

As shown in Figure 12b, under the fixed-*K* method, the energy storage unit continuously operates at high output, and its SOC decreases to the lower operating limit of 0.1 at t = 47 s. Since no SOC recovery constraint is imposed, the SOC then remains at the lower bound. In contrast, under the proposed adaptive control strategy, the SOC changes more smoothly and remains in a more favorable operating range throughout the frequency regulation process. These results confirm that the proposed strategy not only improves frequency support performance but also enhances the sustainability of energy storage participation.

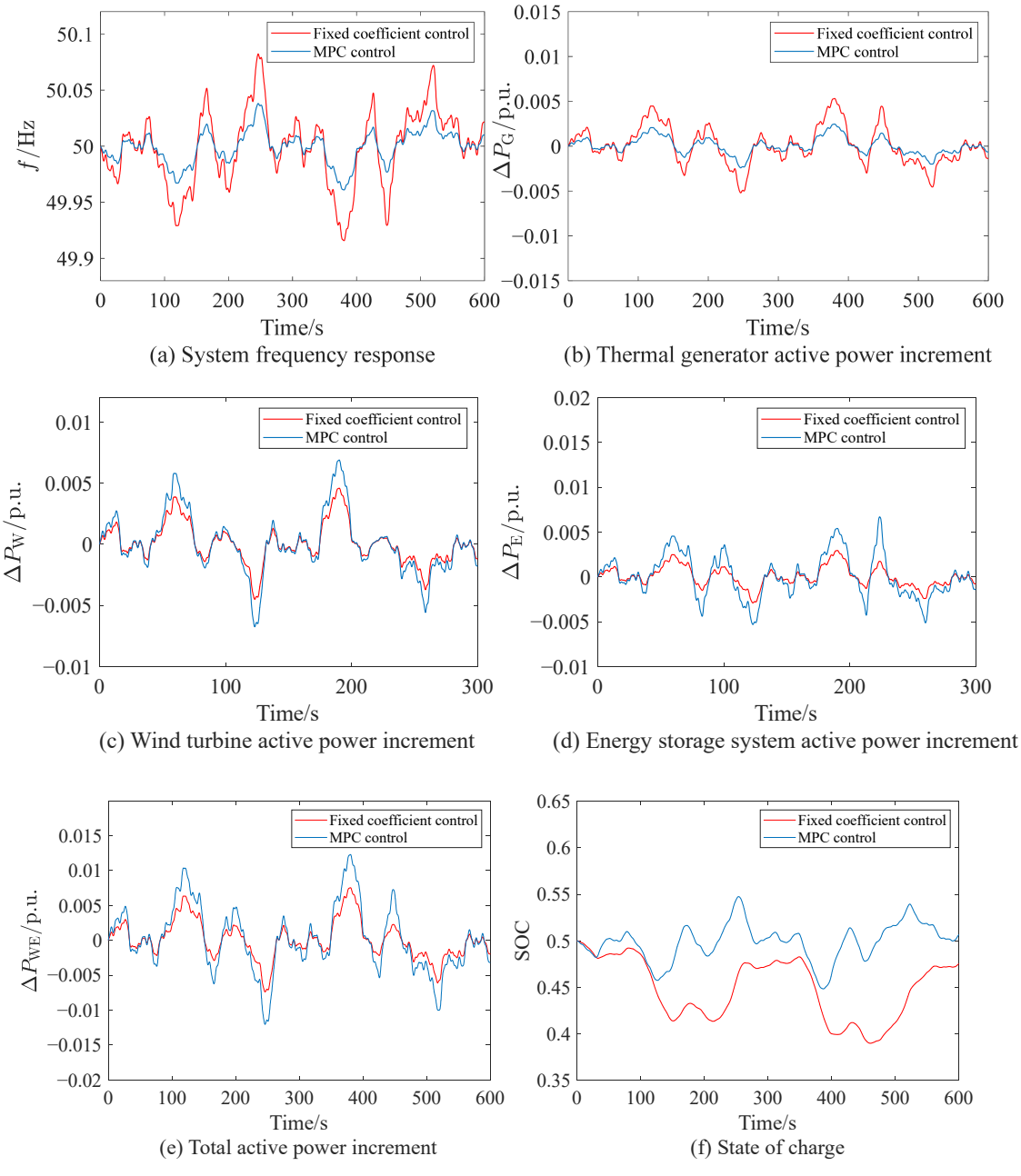
3.4. Validation of the MPC-Based Wind–Storage Power Allocation Strategy

As shown in Figures 13 and 14, a 600 s simulation was conducted under continuously varying wind speed and random load disturbance within ±0.02 p.u. to further evaluate the proposed MPC-based wind–storage power allocation strategy. The dynamic responses of the wind turbine and the energy storage unit under the fixed-coefficient strategy and the proposed MPC-based strategy were compared.



(a) Continuous random wind speed (b) Continuous random load

Figure 13. Continuous random load disturbance under variable wind speed conditions.



(a) System frequency response (b) Thermal generator active power increment

(c) Wind turbine active power increment (d) Energy storage system active power increment

(e) Total active power increment (f) State of charge

Figure 14. Simulation results under continuous random load disturbance.

As shown in Figure 14a, under the fixed-coefficient control strategy, the system frequency fluctuates over a relatively wide range. After the MPC strategy is adopted, the frequency variation is effectively confined within 49.95–50.05 Hz. This result indicates that the MPC-based strategy can better suppress frequency fluctuations under continuously varying operating conditions.

As shown in Figure 14c,d, when the wind speed decreases to about 7.5 m/s at approximately t = 440 s, the available rotor kinetic energy margin of the wind turbine becomes limited. Under the fixed-coefficient strategy, the wind turbine is more prone to rotor speed constraint violation and output oscillation. By contrast, under the proposed MPC-based strategy, the active power command of the wind turbine is reduced in advance, while the energy storage unit is dispatched to increase its output rapidly to compensate for the power deficit. Consequently, the power transition between the two units becomes smoother, and the oscillation risk of the wind turbine is mitigated effectively.

As shown in Figure 14e, under fixed-coefficient control, the peak total active power support of the wind–storage system is only about 0.007 p.u., which accounts for approximately 35% of the system power deficit. In comparison, under the proposed MPC-based strategy, the peak total support increases to about 0.013 p.u. This indicates that the proposed method can exploit the regulation potential of the wind–storage hybrid system more fully and enhance system inertial support more rapidly.

As shown in Figure 14f, compared with the fixed-coefficient control strategy, the SOC of the energy storage unit under MPC remains around 0.5 with relatively small fluctuations, showing a smoother overall trajectory. This result suggests that the proposed strategy improves not only the frequency regulation effect but also the continuity and maintainability of storage participation during primary frequency regulation.

4. Discussion

The above results validate the main working hypothesis of this study, namely that the frequency regulation performance of a wind–storage hybrid system can be improved when the response capabilities of the wind turbine and energy storage are coordinated according to turbine operating conditions, rotor kinetic energy margin, and storage SOC. The simulation results show that neither a purely fixed-coefficient strategy nor an unconstrained variable-coefficient strategy can simultaneously guarantee strong frequency support and safe unit operation. By contrast, the proposed multivariable fuzzy synthetic inertia control with rotor-speed safety constraints achieves a better balance between transient support capability and operational security.

For the wind turbine subsystem, the results indicate that simply increasing inertial response is not sufficient, because excessive kinetic energy release may cause rotor-speed violation and degrade the later-stage frequency recovery performance. This observation is consistent with the physical limitation that the DFIG frequency support capability depends strongly on the available rotor kinetic energy margin. Therefore, the nonlinear attenuation mechanism introduced in this study is essential, because it enables the controller to exploit the turbine support potential under favorable conditions while withdrawing support in a timely manner near the safety boundary. From this perspective, the proposed strategy extends conventional fixed-parameter synthetic inertia control by embedding state awareness into the coefficient regulation process.

For the energy storage subsystem, the comparison between fixed-K control and adaptive control demonstrates that frequency regulation performance should not be evaluated only by the initial response speed. Although fixed-K control can provide rapid support, it tends to deplete the storage capacity prematurely, which weakens the continuity of subsequent support. The proposed adaptive droop strategy addresses this issue by adjusting the storage

output according to SOC, thereby maintaining both dynamic response capability and energy availability. This feature is particularly important for sustained or repeated disturbances, where the long-term availability of storage support becomes as important as its short-term response.

The results obtained under continuously varying wind speed further show that coordinated optimization at the system level is necessary. Local control alone cannot fully resolve the conflict between turbine rotor-speed recovery and storage output continuity, especially when wind speed decreases and the turbine support margin becomes insufficient. The MPC framework improves this coordination by predicting the future system trend and redistributing the power command between the wind turbine and energy storage unit in advance. As a result, the proposed method not only suppresses frequency fluctuations more effectively but also mitigates abrupt power transitions and reduces the risk of secondary frequency deterioration.

Compared with previously reported wind-storage coordinated frequency regulation approaches based on fixed inertia or droop settings, single-layer fuzzy control, or direct storage assistance, the present method provides a more integrated control structure by combining local adaptive response and upper-layer rolling optimization. In particular, the proposed strategy explicitly considers the variation in turbine regulation capability across different wind speed regions and the sustainable support capability of storage under SOC constraints. This explains why the method exhibits superior performance in both transient frequency support and coordinated power allocation.

Although the present results are promising, they are still obtained from simulation on a benchmark two-area system under several simplifying assumptions, including simplified converter dynamics, ideal communication conditions, and an equivalent supercapacitor model. For practical deployment, further work is needed to investigate parameter sensitivity, communication delay, measurement noise, and the applicability of the proposed strategy in larger grid models and hardware-in-the-loop environments. In addition, future studies may incorporate economic objectives, storage degradation costs, and multiple wind farms or heterogeneous storage devices to further improve the engineering value of the coordinated control framework.

It should also be noted that the present work focuses on the mechanism analysis and time-domain validation of a hierarchical nonlinear coordinated control strategy, which involves fuzzy inference, operating-region-dependent logic, SOC-based adaptive droop regulation, and constrained rolling optimization. Within this framework, key quantities such as the attenuation parameter μ, the SOC thresholds, and the MPC weighting parameters are treated as preset design parameters of the corresponding control laws and are determined before the system-level validation studies. Accordingly, the main objective of the present study is to evaluate the effectiveness of the proposed coordinated control strategy under the selected design settings. A full small-signal stability analysis around a single operating point, as well as an exhaustive system-level sensitivity study of all preset design parameters, is beyond the present scope and will be further investigated in future work.

5. Conclusions

To address the challenges of coordinated control and power allocation for a wind–storage hybrid system participating in grid primary frequency regulation under high renewable energy penetration, an integrated optimization method incorporating multivariable fuzzy logic and model predictive control is proposed in this paper. The results confirm that the proposed method provides a coordinated and state-aware control framework for wind–storage primary frequency regulation, with consistency across multi-region operating adaptation, local adaptive support, and upper-layer rolling power allocation. On the basis of mechanism analysis and simulation validation of the coordinated frequency regulation process of the wind–storage hybrid system, the main conclusions can be drawn as follows:

The proposed variable-coefficient fuzzy logic control strategy considering rotor speed safety constraints can dynamically tune the virtual inertia and droop coefficients of the wind turbine according to the system frequency condition and the available rotor kinetic energy margin. Moreover, the introduced nonlinear safety attenuation mechanism compensates for the tendency of excessive response under extreme disturbances, thereby maximizing the transient frequency support potential while effectively preventing turbine disconnection caused by rotor stall or overspeed.

The deployment of the energy storage unit markedly enhances the frequency support capability of the system. Furthermore, the Logistic-function-based adaptive control strategy provides more effective SOC management for the energy storage unit, thereby allowing its output to be adjusted in real time throughout the frequency regulation process.

Under fluctuating wind speed conditions and continuous random load disturbances, the constructed MPC-based power optimization allocation framework performs multi-variable long-horizon rolling prediction, proactively issues withdrawal commands when the rotor kinetic energy of the wind turbine becomes insufficient, and simultaneously dispatches the energy storage system to provide power compensation. As a result, the proposed framework improves the frequency regulation performance while achieving a more reasonable power allocation between the wind turbine and the energy storage unit.

Author Contributions: Conceptualization, T.C. and Y.S.; methodology, Y.S.; software, Y.S.; validation, T.C. and Y.S.; formal analysis, Y.S.; investigation, Y.S.; resources, Y.S.; data curation, Y.S.; writing—original draft preparation, Y.S.; writing—review and editing, T.C.; visualization, T.C.; supervision, T.C. All authors have read and agreed to the published version of the manuscript.

Funding: This research was funded by the National Natural Science Foundation of China (NSFC) under the project titled "Research on Parallel Computing Methods for Holomorphic Embedding of Power Flow in Large-Scale AC/DC Power Grids," with the project number 52077029.

Data Availability Statement: The original contributions presented in this study are included in the article. Further inquiries can be directed to the corresponding author.

Conflicts of Interest: The authors declare no conflicts of interest. The funders had no role in the design of the study; in the collection, analyses, or interpretation of data; in the writing of the manuscript; or in the decision to publish the results.

Nomenclature

The main symbols used in this manuscript are summarized as follows:

K_b	Virtual inertia control coefficient of the wind turbine
K_p	Virtual droop control coefficient of the wind turbine
K_E	Virtual droop control coefficient of the energy storage unit
E_m	Available rotor kinetic energy margin
K'_b	Initial virtual inertia coefficient obtained by fuzzy inference
K'_p	Initial virtual droop coefficient obtained by fuzzy inference
$S(\omega_r)$	Nonlinear safety attenuation function
μ	Penalty adjustment coefficient in the safety attenuation function
K_c	Charging control coefficient of the energy storage unit
K_d	Discharging control coefficient of the energy storage unit
α	Weighting coefficient of the frequency deviation term
β	Weighting coefficient of the wind turbine control increment term
γ	Weighting coefficient of the storage control increment term
N_p	Prediction horizon of MPC
N_c	Control horizon of MPC

Appendix A

Appendix A provides the complete fuzzy rule base of the proposed controller. In the rule tables, E_m, $d\Delta f/dt$, and Δf are the three fuzzy inputs, while K'_b and K'_p are the two fuzzy outputs.

Table A1. Complete fuzzy rule base of the proposed fuzzy controller.

E_m	$d\Delta f/dt$	Δf	K'_b	K'_p
VS	VS	VS	VS	VS
VS	VS	S	VS	VS
VS	VS	M	VS	VS
VS	VS	L	VS	S
VS	VS	VL	VS	S
VS	S	VS	VS	VS
VS	S	S	VS	VS
VS	S	M	VS	VS
VS	S	L	VS	S
VS	S	VL	VS	S
VS	M	VS	VS	VS
VS	M	S	VS	VS
VS	M	M	VS	VS
VS	M	L	VS	S
VS	M	VL	VS	S
VS	L	VS	S	VS
VS	L	S	S	VS
VS	L	M	S	VS
VS	L	L	S	S
VS	L	VL	S	S
VS	VL	VS	S	VS
VS	VL	S	S	VS
VS	VL	M	S	VS
VS	VL	L	S	S
VS	VL	VL	S	S
S	VS	VS	VS	VS
S	VS	S	VS	VS
S	VS	M	VS	S
S	VS	L	VS	M
S	VS	VL	VS	M
S	S	VS	S	VS
S	S	S	S	VS
S	S	M	S	S
S	S	L	S	M
S	S	VL	S	M
S	M	VS	S	VS
S	M	S	S	VS
S	M	M	S	S
S	M	L	S	M
S	M	VL	S	M
S	L	VS	M	VS
S	L	S	M	VS
S	L	M	M	S
S	L	L	M	M
S	L	VL	M	M
S	VL	VS	M	VS
S	VL	S	M	VS
S	VL	M	M	S
S	VL	L	M	M

Table A1. *Cont.*

S	VL	VL	M	M
M	VS	VS	S	VS
M	VS	S	S	S
M	VS	M	S	M
M	VS	L	S	L
M	VS	VL	S	L
M	S	VS	S	VS
M	S	S	S	S
M	S	M	S	M
M	S	L	S	L
M	S	VL	S	L
M	M	VS	M	VS
M	M	S	M	S
M	M	M	M	M
M	M	L	M	L
M	M	VL	M	L
M	L	VS	L	VS
M	L	S	L	S
M	L	M	L	M
M	L	L	L	L
M	L	VL	L	L
M	VL	VS	L	VS
M	VL	S	L	S
M	VL	M	L	M
M	VL	L	L	L
M	VL	VL	L	L
L	VS	VS	S	S
L	VS	S	S	M
L	VS	M	S	L
L	VS	L	S	VL
L	VS	VL	S	VL
L	S	VS	M	S
L	S	S	M	M
L	S	M	M	L
L	S	L	M	VL
L	S	VL	M	VL
L	M	VS	L	S
L	M	S	L	M
L	M	M	L	L
L	M	L	L	VL
L	M	VL	L	VL
L	L	VS	VL	S
L	L	S	VL	M
L	L	M	VL	L
L	L	L	VL	VL
L	L	VL	VL	VL
L	VL	VS	VL	S
L	VL	S	VL	M
L	VL	M	VL	L
L	VL	L	VL	VL
L	VL	VL	VL	VL
VL	VS	VS	S	S
VL	VS	S	S	M
VL	VS	M	S	L
VL	VS	L	S	VL

Table A1. *Cont.*

VL	VS	VL	S	VL
VL	S	VS	M	S
VL	S	S	M	M
VL	S	M	M	L
VL	S	L	M	VL
VL	S	VL	M	VL
VL	M	VS	L	S
VL	M	S	L	M
VL	M	M	L	L
VL	M	L	L	VL
VL	M	VL	L	VL
VL	L	VS	VL	S
VL	L	S	VL	M
VL	L	M	VL	L
VL	L	L	VL	VL
VL	L	VL	VL	VL
VL	VL	VS	VL	S
VL	VL	S	VL	M
VL	VL	M	VL	L
VL	VL	L	VL	VL
VL	VL	VL	VL	VL

References

1. Attya, A.B.T.; Dominguez-Garcia, J.L. Insights on the provision of frequency support by wind power and the impact on energy systems. *IEEE Trans. Sustain. Energy* **2017**, *9*, 719–728. [CrossRef]
2. Fu, Y.; Zhang, X.; Hei, Y.; Wang, H. Active participation of variable speed wind turbine in inertial and primary frequency regulations. *Elect. Power Syst. Res.* **2017**, *147*, 174–184. [CrossRef]
3. Van de Vyver, J.; de Kooning, J.D.; Meersman, B.; Vandevelde, L.; Vandoorn, T.L. Droop control as an alternative inertial response strategy for the synthetic inertia on wind turbines. *IEEE Trans. Power Syst.* **2015**, *31*, 1129–1138. [CrossRef]
4. Wang, S.; Tomsovic, K. Fast frequency support from wind turbine generators with auxiliary dynamic demand control. *IEEE Trans. Power Syst.* **2019**, *34*, 3340–3348. [CrossRef]
5. Guo, Y.; Bao, W.; Ding, L.; Liu, Z.; Kheshti, M.; Wu, Q.; Terzija, V. Analytically derived fixed termination time for stepwise inertial control of wind turbines—Part II: Application strategy. *Int. J. Electr. Power Energy Syst.* **2020**, *121*, 106106. [CrossRef]
6. Rapizza, M.R.; Canevese, S.M. Fast frequency regulation and synthetic inertia in a power system with high penetration of renewable energy sources: Optimal design of the required quantities. *Sustain. Energy Grids Netw.* **2020**, *24*, 100407. [CrossRef]
7. Bao, W.; Ding, L.; Liu, Z.; Zhu, G.; Kheshti, M.; Wu, Q.; Terzija, V. Analytically derived fixed termination time for stepwise inertial control of wind turbines—Part I: Analytical derivation. *Int. J. Electrical Power Energy Syst.* **2020**, *121*, 106120. [CrossRef]
8. Fu, Y.; Wang, Y.; Zhang, X. Integrated wind turbine controller with virtual inertia and primary frequency responses for grid dynamic frequency support. *IET Renew. Power Gener.* **2017**, *11*, 1129–1137. [CrossRef]
9. Lao, H.; Zhang, L.; Zhao, T.; Zou, L. Innovated inertia control of DFIG with dynamic rotor speed recovery. *CSEE J. Power Energy Syst.* **2020**, *8*, 1417–1427. [CrossRef]
10. Yu, L.; Wu, J.; Cheng, Y.; Meng, G.; Chen, S.; Lu, Y.; Xu, K. Control Strategy for Wind Farms-Energy Storage Participation in Primary Frequency Regulation Considering Wind Turbine Operation State. *Energies* **2024**, *17*, 3547. [CrossRef]
11. Chen, C.; Li, L. Frequency Regulation Adaptive Control Strategy of Wind Energy Storage System for Wind Speed Uncertainty. *Energies* **2024**, *17*, 2523. [CrossRef]
12. Phung, B.N.; Wu, Y.-K.; Pham, M.-H. Coordinated Frequency Regulation between DFIG-VSWTs and BESS Hybrid Systems. *Energies* **2024**, *17*, 3099. [CrossRef]
13. Zhang, X.; Qin, S.; Chen, C.; Zhang, Y.; Hao, S.; Wu, Q. Wind turbine storage joint frequency modulation control strategy considering the balance of energy storage charge and discharge. *Power Syst. Technol.* **2024**, *48*, 1938–1946.
14. Shu, H.; Dong, H.; Wang, G.; Chen, J.; Shi, B.; Tang, Y. Wind-storage coordinated control strategy for inertia enhancement of high ratio renewable energy power systems. *J. Energy Storage* **2024**, *97*, 112998. [CrossRef]
15. Yao, Y.; Shi, Y.; Chen, M.; Xu, B.; Lei, Z.; Gao, W.; Li, D. Frequency regulation strategy of wind storage hybrid system based on effective inertia margin. *Int. J. Electr. Power Energy Syst.* **2025**, *173*, 111376. [CrossRef]

16. Niu, G.; Hu, L.; Zheng, N.; Ji, Y.; Wu, M.; Shi, P.; Yan, X. Adaptive Primary Frequency Regulation Control Strategy for Doubly Fed Wind Turbine Based on Hybrid Ultracapacitor Energy Storage and Its Performance Optimization. *Electronics* **2025**, *15*, 182. [CrossRef]
17. Venkat, A.N.; Hiskens, I.A.; Rawlings, J.B.; Wright, S.J. Distributed MPC Strategies With Application to Power System Automatic Generation Control. *IEEE Trans. Control. Syst. Technol.* **2008**, *16*, 1192–1206. [CrossRef]
18. Liu, X.; Zhang, Y.; Lee, K.Y. Coordinated Distributed MPC for Load Frequency Control of Power System With Wind Farms. *IEEE Trans. Ind. Electron.* **2017**, *64*, 5140–5150. [CrossRef]
19. Khalid, M.; Savkin, A.V. An optimal operation of wind energy storage system for frequency control based on model predictive control. *Renew. Energy* **2012**, *48*, 127–132. [CrossRef]
20. Wang, H.; Yang, J.; Chen, Z.; Ge, W.; Ma, Y.; Xing, Z.; Yang, L. Model Predictive Control of PMSG-Based Wind Turbines for Frequency Regulation in an Isolated Grid. *IEEE Trans. Ind. Appl.* **2018**, *54*, 3077–3089. [CrossRef]
21. Wang, X.; Yang, D. Adaptive speed recovery strategy of doubly-fed induction generator based on variable PI control coefficient. *Trans. China Electrotech. Soc.* **2023**, *38*, 41204129. (In Chinese) [CrossRef]
22. Peng, B.; Ma, X.; Ma, X.; Tian, C. Fuzzy-based coordinated control and parameter correction strategy for speed controller of PMSG wind turbine in frequency response. *Energy Rep.* **2023**, *9*, 558–566. [CrossRef]
23. Yang, D.; Jin, Z.; Zheng, T.; Jin, E. An adaptive droop control strategy with smooth rotor speed recovery capability for type III wind turbine generators. *Int. J. Electr. Power Energy Syst.* **2022**, *135*, 107532. [CrossRef]
24. Tu, S.; Zhang, B.; Jin, X. Research on DFIG-ES system to enhance the fast-frequency response capability of wind farms. *Energies* **2019**, *12*, 3581. [CrossRef]
25. Cheng, Y.; Sun, H.; Zhang, Y.; Xu, S.; Zhao, B.; Vorobev, P.; Terzija, V. A consecutive power dispatch in wind farms to mitigate secondary frequency dips. *Int. J. Electr. Power Energy Syst.* **2024**, *158*, 109939. [CrossRef]

Disclaimer/Publisher's Note: The statements, opinions and data contained in all publications are solely those of the individual author(s) and contributor(s) and not of MDPI and/or the editor(s). MDPI and/or the editor(s) disclaim responsibility for any injury to people or property resulting from any ideas, methods, instructions or products referred to in the content.